Postprint of: Szypulski D., Fotyga G., de la Rubia V., Mrozowski M., A Subspace-Splitting Moment-Matching Model-Order Reduction Technique for Fast Wideband FEM Simulations of Microwave Structures, IEEE Transactions on Microwave Theory and Techniques, vol. 68, no. 8 (2020), pp. 3229-3241, DOI: 10.1109/TMTT.2020.3001627

A Subspace-Splitting Moment-Matching Model-Order Reduction Technique for Fast Wideband FEM Simulations of Microwave Structures

Damian Szypulski, *Student Member, IEEE*, Grzegorz Fotyga, *Member, IEEE*, Valentín de la Rubia and Michal Mrozowski, *Fellow, IEEE*

***Abstract*—This article describes a novel model-order reduction (MOR) approach for efficient wide frequency band finite element method (FEM) simulations of microwave components. It relies on the splitting of the system transfer function into two components: a singular one that accounts for the in-band system poles, and a regular part that has no in-band poles. In order to perform this splitting during the reduction process, the projection basis is formed of two sets of orthogonal vectors that must be computed in sequence. The first set to be computed consists of the in-band eigenvectors, which are associated with the dynamics of the electromagnetic field, while the second set uses the block moments of the original system, that are computed in the orthogonal complement to the subspace spanned by the in-band eigenvectors. The advantage of this method is that it results in a more compact reduced-order model than a method that employs only moment matching for the projection basis computations.**

***Index Terms*—Computer-aided engineering, design automation, error analysis, finite-element methods, Galerkin method, microwave circuits, reduced basis methods, reduced-order systems.**

I. Introduction

FULL-wave electromagnetic simulations by means of numerical methods, such as the finite element method (FEM) and the finite difference method, play crucial roles in the design of microwave devices. However, if the analysis involves investigating the electromagnetic behavior of the structure in a wide frequency band, the simulation can become extremely time-consuming, since it will require the solution of a very large linear system of equations at each of the frequency points considered.

Manuscript received Month DD, YYYY; revised Month DD, YYYY; accepted Month DD, YYYY. Date of publication Month DD, YYYY; date of current version Month DD, YYYY. This work was supported in part by the "EDISOn–Electromagnetic Design of flexIble SensOrs" Project, Agreement POIR.04.04.00-00-1DC3/16-00 date December 6, 2016, within the TEAM-TECH Program of the Foundation for Polish Science co-financed by the European Union under the European Regional Development Fund, Smart Growth Operational Program 2014-2020 (*Corresponding author: Damian Szypulski.*)

D. Szypulski, G. Fotyga, and M. Mrozowski are with the Faculty of Electronics, Telecommunications, and Informatics, Gdańsk University of Technology, 80-233 Gdańsk, Poland (e-mail: damian.szypulski@pg.edu.pl; grzfotyg@pg.edu.pl; m.mrozowski@ieee.org).

V. de la Rubia is with the Departamento de Matemática Aplicada a las TIC, ETSI de Telecomunicación, Universidad Politécnica de Madrid, 28040 Madrid, Spain (e-mail: valentin.delarubia@upm.es).

Digital Object Identifier XXXXXXXXXXXXX

Since the early 1990s, numerous numerical techniques have been proposed to rapidly compute the scattering matrix of devices at many frequency points—so-called fast-frequency sweep methods. Such techniques are of two types: data-driven and model-driven. In the former, the formula for a rational interpolating function that approximates the original transfer function is sought, based on the response of the original model, computed at carefully selected frequency points. Examples of data-driven techniques can be found in [1]–[6].

On the other hand, model-driven approaches use the concept of model-order reduction (MOR) and transform the original system of equations (the full-order model, FOM) to a so-called reduced-order model (ROM). In MOR, the solution is sought in a low-dimensional subspace spanned by a suitable chosen set of vectors $\mathbf{Q}$. The original problem is then projected onto this subspace using the Galerkin procedure, resulting in the ROM. Since the size of the projection space is small, the number of degrees of freedom in the ROM is a few orders of magnitude smaller than in the FOM, allowing fast computation of the system transfer function at many frequency points. There are two main types of MOR methodologies. The first, referred to as reduced-basis methods (RBM) [7], [8], takes advantage of the fact that a small number of field solutions (called *snapshots*) are sufficient to represent the fundamental dynamics of the original model. These snapshots are assembled and orthogonalized, forming the orthonormal projection basis $\mathbf{Q}$. RBM generates very compact ROMs, but requires the solution of the original FEM system of equations at each snapshot frequency point, which can be time consuming, especially for wideband analysis. This drawback is eliminated in MOR techniques based on the moment-matching property, where just one or a few FEM solutions are needed, since the original and reduced system transfer function themselves and their derivatives are matched at one specified frequency [9]–[11], or at just a few points [12]–[15]. In this case, the projection basis $\mathbf{Q}$ is composed of the subsequent block moments of the original model. The first model-driven techniques were introduced into electronic circuit analysis in the early 1990s with the development of the asymptotic waveform evaluation (AWE) [11], in which the original and reduced block moments are matched in an explicit way. However, the reduced models computed using AWE are prone to numerical instability.

As a remedy, modifications of AWE—such as the Galerkin asymptotic waveform evaluation (GAWE) [16], the multipoint Galerkin asymptotic waveform evaluation (MGAWE) [17], the adaptive multiexpansion frequencies approach [18], and the well-conditioned asymptotic waveform evaluation (WCAWE) [19]—were proposed. In order to ensure the passivity of the reduced-order systems, the passive reduced-order interconnect macromodeling algorithm (PRIMA) was put forward [20]. PRIMA is suitable for first-order systems. For FEM analysis, techniques that can handle second-order systems are especially attractive. Efficient nodal-order reduction (ENOR) [10] was one of the first such techniques, but it unfortunately suffers from similar instability issues as AWE does.

A remarkable single-point moment-matching based technique for second-order systems called the second-order Arnoldi method for passive-order reduction (SAPOR) was proposed in [9] and [21]. It is stable, proven to be passive, and the moments of the reduced model are accurately matched with the moments of the original model. However, the projection basis generated by SAPOR (and, in effect, the reduced model itself) tend to be excessively large. What is more, this approach is better for narrowband simulations, since the reduction error is low only in the vicinity of the expansion point, whereas at the sides of the frequency band of interest it can be large. The width of the frequency band can be extended using multipoint moment-matching approaches, such as [14], [15], [17], [18]. However, these involve an extra cost associated with the factorization of the large FEM matrix at each expansion point. The projection basis resulting from multipoint moment-matching techniques can also be large.

This paper presents a novel compact model-order reduction approach called subspace-splitting moment-matching MOR (SSMM-MOR), which is inspired by the idea presented in [22], and extends our recent preliminary work [23]. The key concept is the same as in the recently proposed compact reduced-basis method (CRBM) [22] and we take advantage of it in this work: to decompose the projection spaces into two subspaces, namely, a singular subspace and a regular subspace. Like in CRBM, the regular projection subspace is generated in such a way that each of its vectors is orthogonal in the energy sense to the subspace used to represent the singular part. In this work, we show that this results in automated splitting of the reduced system transfer function into singular and regular parts. These two parts can then be considered independent one of the other, and this fact is essential for developing a new moment-matching MORe technique we propose in this paper. The singular part tends to be highly nonlinear and is approximated using the subspace composed of the eigenvectors associated with the system poles in the frequency band of interest. These describe the natural oscillating dynamics of the electromagnetic field. On the other hand, as already noted in [22], the transfer function associated with the regular part is rather smooth and it can thus be approximated using a different basis. In [22] snapshots were used to this effect - like in RBM, here we propose the subspace to be composed of just a few block moments of the original model computed using a modified SAPOR algorithm.

In effect, the resultant reduced-order model is accurate for wide-frequency band analysis. SSMM-MOR usually requires the original FEM system matrix to be factorized only once in order to compute eigenvectors and block moments. By the same token, the entire process is controlled by an efficiently computed error estimator that assesses the error introduced by the reduction process and effectively serves as stopping criterion.

II. Finite element method background

We consider a source-free and lossless computational domain $\Omega \subset \mathbb{R}^3$, with the boundary made of a perfect electric conductor (denoted by Γ_E) and the cross-sections of waveguide ports (denoted by Γ_P^p, with $p = 1, \dots n_p$), where n_p is the number of ports. In order to compute the scattering parameters of the microwave structures using the finite element method (FEM), we must first consider the following boundary value problem (BVP):

$$\begin{aligned} \nabla \times ({\mu_r}^{-1} \nabla \times \vec{E}) - k_0^2 \epsilon_r \vec{E} = 0 \qquad & \text{in } \Omega, \\ (\mu_r^{-1} \nabla \times \vec{E}) \times \hat{n} + j k_0 \eta_0 \vec{h}_{pk} = 0 \qquad & \text{on } \Gamma_P^p, \\ \vec{E} \times \hat{n} = 0 \qquad & \text{on } \Gamma_E, \end{aligned} \tag{1}$$

where $\hat{n}$ is the outward normal unit vector on the boundary of Ω, $\vec{E}$ is the electric field, j is the imaginary unit, k_0 is the wavenumber, ϵ_r and μ_r are the relative permittivity and permeability of the medium, respectively, η_0 is the characteristic impedance of free-space, and $\vec{h}_{pk}$ is the normalized pattern of the tangential magnetic field associated with k-th mode at the p-th port. The overall number of modes in the analysis is n_m.

A weak formulation of the above BVP is obtained by considering a vector testing function $\vec{W}$ (see [14], [24] for details). The FEM formulation begins with the discretization of the computational domain—in our case, by means of curvilinear tetrahedrons [25]. Next, the set of the second-order hierarchical vector basis functions in each tetrahedron is defined [26]. The electric field and the testing function are written down as follows:

$$\begin{aligned} \vec{E} &= \sum_{k=1}^{n} e_k \vec{T}_k \\ \vec{W} &= \sum_{k=1}^{n} w_k \vec{T}_k, \end{aligned} \tag{2}$$

where $\vec{T}_k$ are basis functions, n is the number of applied functions and e_k, w_k are coefficients. Following the standard FEM procedure applied to the weak form, we obtain the following n-dimensional second-order input–output system of equations:

$$\begin{aligned} (\mathbf{\Gamma} + s^2 \mathbf{C}) \mathbf{E}(s) &= s \mathbf{B} \mathbf{I}_c, \\ \mathbf{U}_v &= \mathbf{B}^H \mathbf{E}, \end{aligned} \tag{3}$$

where $\mathbf{\Gamma}$ and $\mathbf{C} \in \mathbb{R}^{n \times n}$ are the FEM symmetric system matrices, n is the number of FEM degrees of freedom, $s = j\omega/c$ is the complex frequency (with c being the speed of light and ω being the angular frequency), $\mathbf{E} \in \mathbb{C}^{n \times n_m}$ is

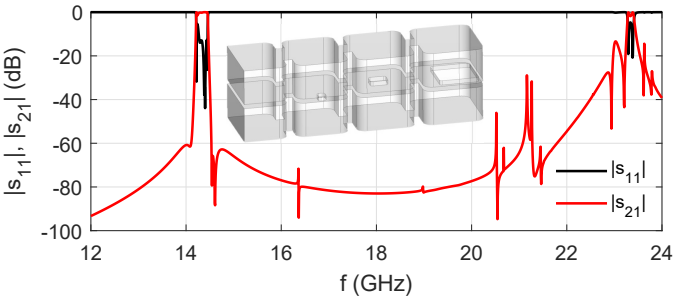

Fig. 1: Scattering parameters and geometry of the folded waveguide filter.

the matrix of unknowns (the FEM basis function coefficients), $\mathbf{U}_v$, $\mathbf{I}_c \in \mathbb{C}^{n_m \times 1}$ are the vectors of amplitudes of the voltage and current waves, respectively, $\mathbf{B} \in \mathbb{C}^{n \times n_m}$ is the normalized matrix associated with the excitation applied to the ports of the structure and $(\cdot)^H$ stands for the conjugate transpose. In order to characterize the microwave structures in terms of the scattering parameters at the specified frequency points in a given frequency band, it is necessary to carry out a frequency sweep in which the system of equations (3) is solved for $s = \{s_1, s_2, \ldots s_{n_f}\}$, and, at each point, the scattering parameters are computed using the formula:

$$\mathbf{S}(s) = 2(\mathbf{I} + \mathbf{Z}(s)^{-1})^{-1} - \mathbf{I}, \tag{4}$$

with $\mathbf{I}$ being the identity matrix, where the impedance matrix $\mathbf{Z}(s)$ is given by:

$$\mathbf{Z}(s) = \mathbf{B}^H(\mathbf{\Gamma} + s^2\mathbf{C})^{-1}s\mathbf{B}. \tag{5}$$

It is important to note that $\mathbf{Z}(s)$ is considered as the transfer function of system (3).

In practice, the frequency sweep process can be memory-demanding and time-consuming, especially when complex devices are being analyzed or optimized in a wide frequency band, or when the goal of the simulation is to predict spurious passbands or the effect of higher-order modes [1]. More precisely, the entire FEM process can be divided into a few steps, the most time-consuming of which are: generation of the tetrahedral mesh, preprocessing, construction of the FEM system of equations (3), and the solution of the resultant system for the specified frequencies. The final step involves symbolic and numerical factorization and solving the system of equations using the factors [27]. To give an idea of the duration of the steps associated with the FEM simulations, we consider a real case: the sixth-order waveguide folded filter [28] shown in Fig. 1. The goal of the simulation is to compute its scattering parameters in the 12–24 GHz band. It is important to note that in this band, five waveguide modes are excited at each of the two ports. The number of excitation vectors is thus $n_m = 10$. The standard FEM formulation [29] results in a system of equations with 359,202 unknowns. The running time of the main FEM steps is summarized in Fig. 2. For simulation of a single frequency point, the mesh generation process is the most time-consuming part. However, if we consider the simulation with 51 points, we can see that numerical factorization is definitely the most demanding part. Thus, in order to speed up the overall FEM analysis of a given frequency band, it is desirable to focus on reducing the frequency sweep time. This problem is addressed in the next section.

III. Classic Moment-Matching Based MOR Approaches

One of the most popular family of techniques for speeding up frequency-domain computational electromagnetic simulations is MOR, the aim of which is to transform the original system of equations to a ROM of the following form:

$$\begin{aligned}(\mathbf{\Gamma}_R + s^2\mathbf{C}_R)\mathbf{E}_R(s) &= s\mathbf{B}_R\mathbf{I}_c,\\ \mathbf{U}_v &= \mathbf{B}_R^H\mathbf{E}_R,\end{aligned} \tag{6}$$

where:

$$\begin{aligned}\mathbf{\Gamma}_R &= \mathbf{Q}^T\mathbf{\Gamma}\mathbf{Q},\\ \mathbf{C}_R &= \mathbf{Q}^T\mathbf{C}\mathbf{Q},\\ \mathbf{B}_R &= \mathbf{Q}^T\mathbf{B},\end{aligned} \tag{7}$$

are reduced system matrices in the sets $\mathbf{\Gamma}_R$, $\mathbf{C}_R \in \mathbb{C}^{v \times v}$, and $\mathbf{B}_R \in \mathbb{C}^{v \times n_m}$. Matrix $\mathbf{Q} \in \mathbb{C}^{n \times v}$ is the orthonormal projection basis, where v denotes the number of vectors in the projection basis. Since the number of unknowns in (6) is much smaller than in (3) ($v \ll n$), the solution and, therefore, the frequency sweep over the specified frequency band in this case is performed much more rapidly, resulting in the reduced transfer function:

$$\mathbf{Z}_R(s) = \mathbf{B}_R^H(\mathbf{\Gamma}_R + s^2\mathbf{C}_R)^{-1}s\mathbf{B}_R, \tag{8}$$

which approximates the original model with sufficient accuracy over the desired frequency range.

As briefly discussed in the introduction, many MOR techniques have been proposed. In this work, we consider SAPOR due to its stability, accuracy and efficiency. For the sake of clarity, we provide an outline of this technique here; a comprehensive description can be found in [9], [21].

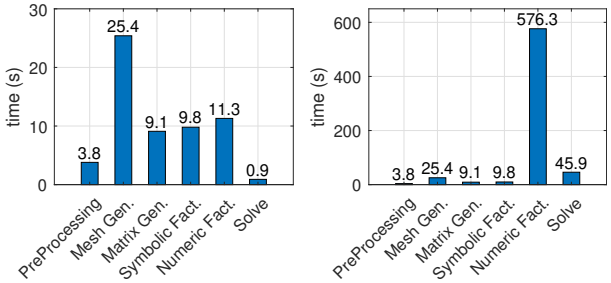

Fig. 2: Simulation times for specific stages of simulation. The first plot corresponds to the simulation of a single frequency point, while the second one to simulation of 51 frequency points. Intel MKL PARDISO [27] was used to solve large systems of linear equations.

A. The SAPOR method

The goal of SAPOR is to generate the orthonormal projection basis $\mathbf{Q}$, which is used to transform the original system (3) to the reduced system (6). The basis $\mathbf{Q}$ is orthonormalized using a numerically stable Krylov subspace method, and is spanned by q moments of $\mathbf{E}(s)$, where q is called the reduction order. Therefore, q moments of the reduced system are matched with the moments of the original one.

In its basic form, and taking into account that the second-order system is of the form of (3)—that is, it has no first-order terms—the SAPOR algorithm is as follows:

1) Equation (3) is shifted using $s = s_0 + \sigma$, resulting in:
$$(\sigma^2\mathbf{C} + \sigma\mathbf{D} + \mathbf{K})\mathbf{E}(\sigma) = \mathbf{B}_0 + \sigma\mathbf{B}_1 \tag{9}$$
where: $\mathbf{D} = 2s_0\mathbf{C}$, $\mathbf{K} = s_0^2\mathbf{C} + \mathbf{\Gamma}$, $\mathbf{B}_0 = s_0\mathbf{B}$, and $\mathbf{B}_1 = \mathbf{B}$.
2) Next, an auxiliary variable is introduced:
$$\mathbf{Z}(\sigma) = \mathbf{B}_1 - \sigma\mathbf{C}\mathbf{E}(\sigma) \tag{10}$$
3) Substituting (10) into (9), we obtain:
$$(\mathbf{I} - \sigma\mathbf{A})\begin{bmatrix}\mathbf{E}\\ \mathbf{Z}\end{bmatrix} = \begin{bmatrix}\mathbf{Q}_0\\ \mathbf{P}_0\end{bmatrix} \tag{11}$$
where $\mathbf{Q}_0$ is the zeroth block moment of $\mathbf{E}$,
$$\mathbf{A} = \begin{bmatrix}-\mathbf{K}^{-1}\mathbf{D} & \mathbf{K}^{-1}\\ -\mathbf{C} & \mathbf{0}\end{bmatrix}, \quad \mathbf{Q}_0 = \mathbf{K}^{-1}\mathbf{B}_0, \tag{12}$$
and:
$$\mathbf{P}_0 = \mathbf{B}_1. \tag{13}$$
4) The block second-order Arnoldi (SOAR) algorithm is used to construct the Krylov subspace: basis $\mathbf{Q} \in \mathbb{C}^{n\times v}$, where $v = qn_m$. What is important, $\mathbf{Q}$ is spanned by the block moments of $\mathbf{E}$ and is orthonormal, where the second-order orthonormalization is performed by means of the Gram-Schmidt approach called SOrth. Pseudocode and the details of these two techniques are provided in [21].
5) Finally, the reduced-order model (6) is generated using the basis $\mathbf{Q}$.

It is remarkable that in the SAPOR process (as in other moment-matching based algorithms), the most time-consuming steps of symbolic and numerical factorization of the original FEM system matrix are performed only once. Computation of each subsequent block moment requires just a single (block) solve of the FEM system of equations using the factors already stored in the memory. SAPOR in most cases therefore outperforms fast-frequency sweep methods that require the system matrix to be factorized many times (at many expansion frequency points); include RBM [7], [30] and data-driven approaches [1]–[6].

B. Error estimator

In order to be able to use SAPOR, we need to assess the error of the ROM. This error estimate can then be used as the stopping criterion for the algorithm [8], [30]–[33].

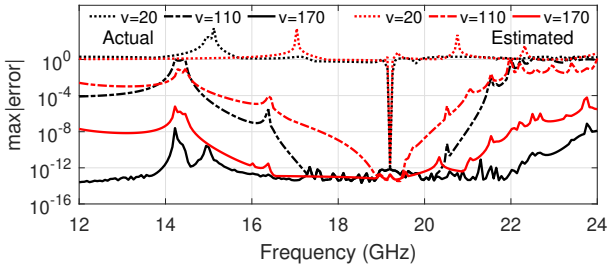

Fig. 3: SAPOR in the analysis of the folded waveguide filter in Fig. 1.

In practice, we do not know the error introduced by the ROM with respect to the original model. To assess this error, we take advantage of an *a posteriori* error estimator. Since the error must be evaluated over the whole frequency bandwidth, it is important that it can be computed extremely rapidly.

We here use a goal-oriented error estimator (described in details in [8]) that considers the interaction of the residual error with the excitation at the ports. It is defined as:
$$e_s(s) = |\mathbf{Z}_p(s)\mathbf{B}^H\mathbf{R}(s)|/|2s\mathbf{Z}_p(s)\mathbf{B}^H\mathbf{B}|,, \tag{14}$$
where $\mathbf{Z}_p(s) = diag[\eta_1(s), \eta_2(s), \ldots, \eta_{n_m}(s)]$ is the impedance normalization matrix, with $\eta_i(s)$ being the impedance of the i-th mode. The residual error $\mathbf{R}(s)$, used in (14), has the form:
$$\mathbf{R}(s) = 2s\mathbf{B} - (\mathbf{\Gamma} + s\mathbf{B}\mathbf{B}^H + s^2\mathbf{C})\mathbf{Q}\bar{\mathbf{E}}_R(s), \tag{15}$$
whereas $\bar{\mathbf{E}}_R(s)$ is the solution of the reduced system of equations:
$$\bar{\mathbf{E}}_R(s) = (\mathbf{\Gamma}_R + s\mathbf{B}_R\mathbf{B}_R^H + s^2\mathbf{C}_R)^{-1}(2s\mathbf{B}_R). \tag{16}$$
In order to efficiently assess the error over the whole frequency band, the formula (14) is transformed to:
$$e_s(s) = |2s\mathbf{Z}_p\mathbf{B}^H\mathbf{B} - \mathbf{Z}_p\mathbf{B}^H\mathbf{\Gamma}\mathbf{Q}\bar{\mathbf{E}}_R(s) - s^2\mathbf{Z}_p\mathbf{B}^H\mathbf{C}\mathbf{Q}\bar{\mathbf{E}}_R(s) - s\mathbf{Z}_p\mathbf{B}^H\mathbf{B}\mathbf{B}^H\mathbf{Q}\bar{\mathbf{E}}_R(s)|/|2s\mathbf{Z}_p(s)\mathbf{B}^H\mathbf{B}|. \tag{17}$$
It is important to underline the fact that the low-order blocks $\mathbf{B}^H\mathbf{B}$, $\mathbf{B}^H\mathbf{\Gamma}\mathbf{Q}$, $\mathbf{B}^H\mathbf{C}\mathbf{Q}$, and $\mathbf{B}^H\mathbf{B}\mathbf{B}^H\mathbf{Q}$ are computed only once, in the so-called *offline* stage. In the *online* stage, the frequency-dependent terms are taken into account to estimate the error in the whole frequency bandwidth. As a result, the error estimation can be evaluated throughout the frequency band with ease.

C. Numerical example

Here, the procedures described in subsections III-A and III-B are used to analyze the folded waveguide filter shown in Fig. 1. Fig. 3 shows the actual and estimated errors; the actual error is defined as:
$$e_{\text{actual}} = \max|S_{\text{MOR}} - S_{\text{REF}}|. \tag{18}$$
S_{MOR} is the scattering matrix obtained using SAPOR, whereas S_{REF} is computed directly with FEM by means of (3)–(4). Three cases are considered, with the number of block

moments in the projection basis $\mathbf{Q}$ equal to $q = \{2, 11, 17\}$, corresponding to $v = \{20, 110, 170\}$, since the number of excitation vectors considered is $n_m = 10$. It can be observed that the original and reduced system transfer functions and their derivatives match in the vicinity of the expansion point, which in this case is 19.2 GHz. Obviously the frequency band in which the actual and estimated errors are at the noise level widens with the number of block moments added to the projection basis. The actual and estimated errors are well correlated, so definition (17) can be used to assess the error introduced by the reduced model.

As can be seen, SAPOR allows us to obtain highly accurate reduced-order models in an efficient and numerically stable way. As shown in [9], [21], the moments of the original and reduced models are matched to the specified reduction order. Stopping can be ensured by using the efficient error estimator defined in (17). However, SAPOR works best for narrowband simulations, since in wideband analysis the error at the sides of the frequency band decreases slowly and high reduction orders are needed to bring it down. Compared to the MOR methods, which have been proven to be optimal or nearly optimal in terms of the projection basis size (such as proper orthogonal decomposition or RBM), SAPOR generates an excessively large projection basis.

IV. Decoupled reduced system transfer function

We now have a closer look at the reduced transfer function of the device, as defined in (8). The reduced blocks of matrices $\mathbf{\Gamma}_R$, $\mathbf{C}_R$, and $\mathbf{B}_R$ are obtained by projecting of the original FEM matrices $\mathbf{\Gamma}$, $\mathbf{C}$, and $\mathbf{B}$ onto a subspace spanned by the vectors of the projection basis $\mathbf{Q}$. The main factor contributing to the size of the projection basis in moment-matching MOR is the highly nonlinear behavior of the system transfer function, where many poles are present in the band of interest. In this case, high-order derivatives (in other words, many moments) are needed to accurately approximate the transfer function in the vicinity of these poles, if indeed convergence is achieved. To reduce the size of the projection basis for moment-matching MOR, increasing the computational efficiency and, at the same time, to prevent the algorithm from numerical stagnation, it is beneficial to decompose the system transfer function into regular and singular parts, and to generate a different projection base for each of them.

To this end, we have to firstly take into account, that the distribution of the electric field $\vec{E}(\omega)$ in the band of interest $\mathcal{B} = [\omega_{min}, \omega_{max}]$ can be decomposed into two parts: a regular one, denoted by $\vec{F}(\omega)$, and a singular one, $\vec{e}_{\mathcal{B}}(\omega)$, standing for the eigenmodes hit in the frequency band of analysis, following the theory provided in [22]. By the same token, we can split the basis for the electric field into two sets of vectors:

$$\mathbf{Q} = [\mathbf{Q}_E, \mathbf{Q}_M], \tag{19}$$

and use $\mathbf{Q}_E$ and $\mathbf{Q}_M$ to span the subspace corresponding to the singular and regular part of the electric field solution. Subspace $\mathbf{Q}_E$ is then composed of the electric field eigenvectors associated with the poles in the band of interest, and represents the natural oscillating dynamics of the electric field in the computational domain. The second part, $\mathbf{Q}_M$, spans whatever else is required to approximate the electric field in the band of interest with high accuracy. While $\mathbf{Q}_E$ is already defined, we are free to choose $\mathbf{Q}_M$. Our goal is to generate $\mathbf{Q}_M$ so that the reduced system transfer function is naturally split into the singular part, with the in-band poles, and the regular part, with no poles inside the band.

$$\mathbf{Z}_R(s) = \mathbf{Z}_E(s) + \mathbf{Z}_M(s). \tag{20}$$

This representation allows deeper insight into the contribution of the regular and singular parts to $\mathbf{Z}_R(s)$. In order to derive the *decoupled* representation of the transfer function $\mathbf{Z}_R(s)$, we have to make sure that $\mathbf{Q}_M$ is constructed from vectors that lie in the orthogonal complement of the subspace spanned by $\mathbf{Q}_E$.

If we consider the FEM system matrix, $\mathbf{\Gamma}$ and $\mathbf{C}$, we can construct the following generalized eigenproblem:

$$\mathbf{\Gamma}\mathbf{Q}_E = \mathbf{C}\mathbf{Q}_E\mathbf{\Lambda}, \tag{21}$$

where $\mathbf{\Lambda}$ is a diagonal matrix containing the eigenvalues corresponding to the resonant frequencies in the band of interest, $\mathcal{B}$, and $\mathbf{Q}_E$ are its corresponding eigenvectors, that represent the singular part of the projection basis (19). Since matrices $\mathbf{\Gamma}$ and $\mathbf{C}$ are symmetric, the eigenvectors are C-orthogonal:

$$\mathbf{C}_E = \mathbf{Q}_E^T\mathbf{C}\mathbf{Q}_E = \mathbf{I}. \tag{22}$$

Left-multiplying (21) by $\mathbf{Q}_E^T$ and substituting (22), we obtain:

$$\mathbf{\Gamma}_E = \mathbf{Q}_E^T\mathbf{\Gamma}\mathbf{Q}_E = \mathbf{\Lambda} \tag{23}$$

Now, since we want $\mathbf{Q}_M$ to be in the orthogonal complement of the subspace spanned by $\mathbf{Q}_E$, we enforce C-orthonormality on the regular part of the projection basis $\mathbf{Q}_M$ with respect to $\mathbf{Q}_E$ vectors. We thus obtain:

$$\begin{aligned} \mathbf{Q}_M^T\mathbf{C}\mathbf{Q}_E &= \mathbf{0} \\ \mathbf{Q}_E^T\mathbf{C}\mathbf{Q}_M &= \mathbf{0}. \end{aligned} \tag{24}$$

Using this orthogonality and left-multiplying (21) by $\mathbf{Q}_M^T$, we obtain:

$$\mathbf{Q}_M^T\mathbf{\Gamma}\mathbf{Q}_E = \mathbf{0}, \tag{25}$$

and similarly:

$$\mathbf{Q}_E^T\mathbf{\Gamma}\mathbf{Q}_M = \mathbf{0}. \tag{26}$$

Finally:

$$\begin{aligned} \mathbf{\Gamma}_M &= \mathbf{Q}_M^T\mathbf{\Gamma}\mathbf{Q}_M \\ \mathbf{C}_M &= \mathbf{Q}_M^T\mathbf{C}\mathbf{Q}_M = \mathbf{I} \end{aligned} \tag{27}$$

since the vectors of $\mathbf{Q}_M$ are enforced to be C-orthonormal. It is important to emphasize that $\mathbf{\Gamma}_M$ is a full matrix, since the vectors in $\mathbf{Q}_M$ are not eigensolutions to (21). To summarize the above formulas, we arrive at the following definitions of the reduced-order model matrices:

$$\mathbf{\Gamma}_R^d = \begin{bmatrix} \mathbf{\Lambda} & \mathbf{0} \\ \mathbf{0} & \mathbf{\Gamma}_M \end{bmatrix}, \tag{28}$$

$$\mathbf{C}_R^d = \begin{bmatrix} \mathbf{I} & \mathbf{0} \\ \mathbf{0} & \mathbf{I} \end{bmatrix}, \tag{29}$$

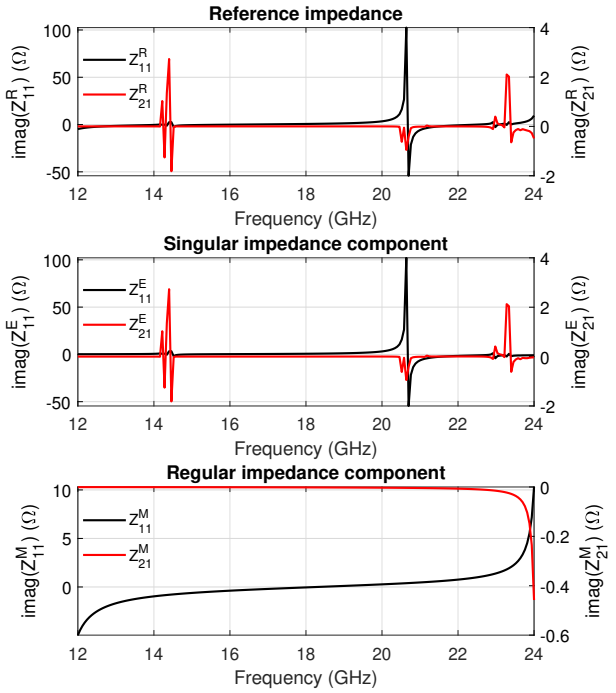

Fig. 4: Process of decoupling the impedance function of the folder filter: singular and regular components of the impedance.

and

$$\mathbf{B}_R^d = \begin{bmatrix} \mathbf{Q}_E^H \mathbf{B} \\ \mathbf{Q}_M^H \mathbf{B} \end{bmatrix} = \begin{bmatrix} \mathbf{B}_E \\ \mathbf{B}_M \end{bmatrix}. \tag{30}$$

As can be seen, the off-diagonal blocks in (28) and (29) are zero matrices, which means that the two blocks associated with the regular and singular parts are decoupled (superscript d corresponds to the decoupling process). The expression for the impedance matrix transfer function, based on the decoupled reduced-model, is thus defined as follows:

$$\mathbf{Z}_R^d(s) = s \begin{bmatrix} \mathbf{B}_E \\ \mathbf{B}_M \end{bmatrix}^H \left(\begin{bmatrix} \mathbf{\Lambda} & \mathbf{0} \\ \mathbf{0} & \mathbf{\Gamma}_M \end{bmatrix} + s^2 \begin{bmatrix} \mathbf{I} & \mathbf{0} \\ \mathbf{0} & \mathbf{I} \end{bmatrix} \right)^{-1} \begin{bmatrix} \mathbf{B}_E \\ \mathbf{B}_M \end{bmatrix}, \tag{31}$$

which can be simplified to:

$$\begin{aligned} \mathbf{Z}_R^d(s) =& s\mathbf{B}_E^H(\mathbf{\Lambda} + s^2\mathbf{I})^{-1}\mathbf{B}_E + \\ & s\mathbf{B}_M^H(\mathbf{\Gamma}_M + s^2\mathbf{I})^{-1}\mathbf{B}_M. \end{aligned} \tag{32}$$

Finally, we obtain the formula for the decoupled impedance matrix transfer function, which is decomposed into the part associated with the singular and regular components, respectively:

$$\mathbf{Z}_R^d(s) = \mathbf{Z}_E^d(s) + \mathbf{Z}_M^d(s). \tag{33}$$

Due to the above decoupling process, we can separately analyze the contribution of the regular and singular parts of the reduced-order model to the system transfer function $\mathbf{Z}_R^d(s)$ that aims to approximate the original impedance matrix transfer function $\mathbf{Z}(s)$. It is now seen that for decoupling all that is needed is the C-orthogonality of $\mathbf{Q}_M$ and $\mathbf{Q}_E$. Part $\mathbf{Q}_M$ can be determined in many ways. One possible approach is to use snapshots and C-orthogonalize them (like in CRBM [22]), but other approaches are also possible and become apparent by examining the frequency behaviour of the two parts of the impedance matrix transfer function.

To this end, we consider the sixth-order folded filter analyzed in Section II. The imaginary part of the transfer function $\mathbf{Z}(s)$ associated with the fundamental waveguide port mode is plotted in Fig. 4. It can be seen that this is a highly nonlinear function. The next plot in Fig. 4 shows the singular part of the impedance, $\mathbf{Z}_E(s)$, which is also a highly nonlinear function. We focus on the regular part of the impedance, namely $\mathbf{Z}_M(s)$, which is shown in the last plot in Fig. 4. This plot makes it clear that, as previously noted in [22], this is indeed a rather smooth function (in contrast to the two previous plots in Fig. 4) that can be approximated using a low-order polynomial, or just a few terms of the Taylor expansion.

This result suggests that, in order to approximate the regular part of the transfer function, we can take advantage of the fact that moment-matching reduction techniques require just one symbolic and one numerical factorization of the FEM system matrix. The derivatives of the transfer function, associated with subsequent moment, are then computed by several solutions of the linear system of equations, which can be done relatively rapidly. However, in order to use this, the moment-matching based model-order reduction procedure needs to be modified to enforce C-orthogonality with respect to the eigenvectors hit in the frequency band of analysis only.

V. Subspace Splitting Moment-Matching Model-Order Reduction Technique

With the conclusions from Sections III and IV, we are now ready to derive the subsequent steps of the novel model-order reduction approach, exploiting subspace splitting. We start the reduction process by computing n_E eigenvectors associated with the resonant frequencies in the band of interest $\mathcal{B}$. We use the shift-and-invert preconditioner and Arnoldi iteration [34] to efficiently find resonances. The original generalized eigenproblem to be solved is defined in (21), which for a single eigenpair takes the form:

$$(\mathbf{\Gamma} - \lambda\mathbf{C})\mathbf{q}_E = 0. \tag{34}$$

Since iterative solvers converge well to large eigenvalues, and the eigenvalues of interest are relatively small, we first perform a spectral transformation to push the eigenvalues we are looking for towards the end of the spectrum and thus enhance the convergence. The spectral transformation affects the eigenvalues but does not affect eigenvectors. This operation transforms the original generalized eigenproblem into the standard eigenproblem:

$$\mathbf{T}\mathbf{q}_E = \gamma\mathbf{q}_E, \tag{35}$$

with $\gamma = (\lambda - \sigma)^{-1}$ and

$$\mathbf{T} = (\mathbf{\Gamma} - \sigma\mathbf{C})^{-1}\mathbf{C}, \tag{36}$$

where $\sigma \neq \lambda$ is a shift. The largest in magnitude eigenvalues γ correspond to the eigenvalues λ of the original problem that are closest to the σ. The eigenvalue we are interested in is

then recovered as $\lambda = \sigma + 1/\gamma$. Very often this method needs just one factorization of the FEM system matrix to find all eigenvalues in the wide frequency band of interest, as can be seen in all considered numerical tests. However, in case the shift-and-invent Arnoldi process does not converge, additional factorizations of system matrix for different shifts have to be computed.

Next, in order to approximate the regular subspace, we use the moment-matching approach, or more precisely the block SOAR and SOrth (Second-order Orthonormalization) methods described in [35]. However, in order to take advantage of the decoupling property of the system transfer function, we need to modify these algorithms to preserve the C-orthogonality of the overall projection basis.

The moment-matching process based on block SOAR does not require any additional factorizations of the system matrix since, in order to compute the zeroth block moment, we use the matrix factors obtained in the previous step to compute the eigenvectors. Each subsequent block moment requires just a single solve of the system of equations using the factors already stored in memory. As shown in Section IV, the regular part of the transfer function is rather smooth, so a small number of block moments suffice to accurately approximate it. This is in contract to the large number of block moments required to match the system transfer function response in wide frequency band of analysis in the original moment-matching algorithm.

For the sake of clarity, we provide here the algorithms of the modified SOAR and SOrth procedures.

1 input: $\mathbf{A}$, $\mathbf{C}$, $\mathbf{Q}_E$, $\mathbf{Q}_0$, $\mathbf{P}_0$, q , n_m
2 output: orthonormal projection basis $\mathbf{Q}_{\text{OUT}}$
3 $\mathbf{H}^E = \mathbf{Q}_E^T \mathbf{C} \mathbf{Q}_0$
4 $\mathbf{Q}_0 = \mathbf{Q}_0 - \mathbf{Q}_E \mathbf{H}^E$
5 $\mathbf{Q}_1 = \text{SOrth}\big(\mathbf{Q}_0, \mathbf{C}\big)$, $\mathbf{P}_1 = \mathbf{P}_0$
6 for $i = 1, 2, \ldots, q$
7 $\begin{bmatrix} \hat{\mathbf{Q}}_{i+1} \\ \hat{\mathbf{P}}_{i+1} \end{bmatrix} = \mathbf{A} \begin{bmatrix} \mathbf{Q}_i \\ \mathbf{P}_i \end{bmatrix}$
8 $\mathbf{H}_i^E = \mathbf{Q}_E^T \mathbf{C} \hat{\mathbf{Q}}_{i+1}$
9 $\mathbf{H}_i = \mathbf{Q}_{1:i}^T \mathbf{C} \hat{\mathbf{Q}}_{i+1}$
10 $\hat{\mathbf{Q}}_{i+1} = \hat{\mathbf{Q}}_{i+1} - \mathbf{Q}_E \mathbf{H}_i^E$
11 $\hat{\mathbf{Q}}_{i+1} = \hat{\mathbf{Q}}_{i+1} - \mathbf{Q}_{1:i} \mathbf{H}_i$
12 $\mathbf{Q}_{i+1} = \text{SOrth}\big(\hat{\mathbf{Q}}_{i+1}, \mathbf{C}\big)$
13 end
14 $\mathbf{Q}_{\text{OUT}} = \text{append}(\mathbf{Q}_E, \mathbf{Q}_{1:q})$,

Algorithm 1: Modified SOAR procedure.

$\mathbf{A}$, $\mathbf{Q}_0$, and $\mathbf{P}_0$ are defined in (12) and (13). Firstly (step 4), the 0-th block moment is C-orthogonalized with respect to the singular part of the projection basis $\mathbf{Q}_E$, using the coefficients computed in step 3. Next, in step 5, the C-orthogonality is enforced among the vectors that form the 0-th block moment, using the modified SOrth procedure. The subsequent block moments are computed in step 7, and they are subject to the C-orthognalization with respect to $\mathbf{Q}_E$ (step 10), as well as the previous block moments (step 11), using the coefficients computed in steps 8 and 9, respectively. In the last step, the singular part of the projection basis is extended by the regular component composed of the subsequent block moments.

1 Input: $\hat{\mathbf{Q}}_m$, $\mathbf{C}$, n_m
2 Output: the C-orthonormal matrix - $\mathbf{Q}_m$
3 set $\hat{\mathbf{Q}}_m = \big[\hat{\mathbf{q}}_1\ \hat{\mathbf{q}}_2\ \ldots\ \hat{\mathbf{q}}_{n_m}\big]$
4 for $i = 1, 2, \ldots, n_m$
5 for $j = 1, 2, \ldots, i-1$
6 $\mathbf{R}_{ji} = \mathbf{q}_j^T \mathbf{C} \hat{\mathbf{q}}_i$
7 $\hat{\mathbf{q}}_i = \hat{\mathbf{q}}_i - \mathbf{R}_{ji} \mathbf{q}_j$
8 end
9 $\mathbf{R}_{ii} = \sqrt{\hat{\mathbf{q}}_i^T \mathbf{C} \hat{\mathbf{q}}_i}$
10 if $\mathbf{R}_{ii} \cong 0$, stop (deflation)
11 $\mathbf{q}_i = \frac{1}{\mathbf{R}_{ii}} \hat{\mathbf{q}}_i$
12 end
13 end
14 $\mathbf{Q}_m = \big[\mathbf{q}_1\ \mathbf{q}_2\ \ldots\ \mathbf{q}_{n_m}\big]$

Algorithm 2: Modified SOrth procedure.

It should be noted that $\hat{\mathbf{q}}_i^T \mathbf{C} \hat{\mathbf{q}}_i$ is positive, since $\mathbf{C}$ is a symmetric positive-definite matrix.

A. The complete SSMM-MOR approach

The proposed subspace-splitting moment-matching (SSMM) model-order reduction algorithm can now be summarized in the following steps:

1) Perform the factorization of the original FEM system matrix at the central frequency point s_c.
2) Compute the eigenvectors associated with the eigenvalues from the frequency band of interest using shift-and-invert transformation (e.g., with the Implicitly Restarted Arnoldi or Lanczos method [36]), with the shift set to the center frequency.
3) Form the singular part of the projection basis $\mathbf{Q}_E$ from the eigenmodes.
4) Using the factors obtained in step 1, generate the 0-th block moment to form the regular part of projection basis $\mathbf{Q}_M$.
5) While the maximum value of the error estimator is above the assumed threshold, repeat: using the factors obtained in step 1, uplift the regular part of projection basis $\mathbf{Q}_M$ with the new block moment.

As noted, the method requires just one symbolic and numerical factorization of the original FEM system matrix to generate both parts of the projection basis. This strategy is efficient even for wide-frequency bands of interest, as shown in the numerical examples considered in Section VI. However, in case single-point moment matching approaches (such as SAPOR) fail to converge, multi-point moment-matching techniques (such as [15], [37]) can be of help.

B. Extension to lossy dielectrics

The proposed SSMM-MOR approach can be used to perform a fast frequency sweep of lossless problems, where the FEM system matrices $\mathbf{\Gamma}$ and $\mathbf{C}$ are real symmetric. In order to apply this method to problems which include lossy dielectrics (with complex permittivity and permeability), the formulas for the decoupled impedance function have to be properly updated, since system matrices in these cases are complex symmetric (non-Hermitian). To this end, C-orthogonality with respect to the pseudoinner product (without complex

conjugate) has to be used. For such problems, we define the following eigenproblem, where the superscript l refers to lossy cases:

$$\mathbf{\Gamma}^l \mathbf{Q}_E^l = \mathbf{C}^l \mathbf{Q}_E^l \mathbf{\Lambda}^l, \tag{37}$$

where $\mathbf{\Lambda}^l$ and $\mathbf{Q}_E^l$ are the eigenvalues and corresponding eigenvectors, respectively. Taking into account the C-orthogonality on the basis of the pseudoinner product of the vectors in both parts of the projection basis $\mathbf{Q}_E^l$ and $\mathbf{Q}_M^l$, normalization of the vectors, as well as the symmetry $\mathbf{\Gamma} = \mathbf{\Gamma}^T$, we get:

$$\begin{aligned}
\mathbf{C}_E^l = (\mathbf{Q}_E^l)^T \mathbf{C}^l \mathbf{Q}_E^l &= \mathbf{I}, \\
\mathbf{\Gamma}_E^l = (\mathbf{Q}_E^l)^T \mathbf{\Gamma}^l \mathbf{Q}_E^l &= \mathbf{\Lambda}^l, \\
(\mathbf{Q}_M^l)^T \mathbf{C}^l \mathbf{Q}_E^l &= \mathbf{0}, \\
(\mathbf{Q}_E^l)^T \mathbf{C}^l \mathbf{Q}_M^l &= \mathbf{0}, \\
(\mathbf{Q}_M^l)^T \mathbf{\Gamma}^l \mathbf{Q}_E^l &= \mathbf{0}, \\
(\mathbf{Q}_E^l)^T \mathbf{\Gamma}^l \mathbf{Q}_M^l &= \mathbf{0}, \\
\mathbf{\Gamma}_M^l &= (\mathbf{Q}_M^l)^T \mathbf{\Gamma}^l \mathbf{Q}_M^l, \\
\mathbf{C}_M^l = (\mathbf{Q}_M^l)^T \mathbf{C}^l \mathbf{Q}_M^l &= \mathbf{I},
\end{aligned} \tag{38}$$

and we finally obtain the formula for the decoupled impedance matrix $\mathbf{Z}_R^l(s)$, for which the SSMM-MOR approach can be utilized, similarly as in the lossless case:

$$\begin{aligned}
\mathbf{Z}_R^l(s) = & s\mathbf{B}_E^H (\mathbf{\Lambda}^l + s^2\mathbf{I})^{-1} \mathbf{B}_E + \\
& s\mathbf{B}_M^H (\mathbf{\Gamma}_M + s^2\mathbf{I})^{-1} \mathbf{B}_M.
\end{aligned} \tag{39}$$

C. Limitations of the SSMM-MOR technique

In order to be able to take advantage of the projection subspace splitting, we have to use the orthogonality property. This implies that we have to restrict FEM formation to cases where the system matrices are frequency-independent. This means that SSMM-MOR is not suitable for FEM simulations with PML or dispersive materials (e.g., ferrites).

Also, we can only deal with problems that lead to both constant and second-order frequency terms in FEM equations. More complicated forms, for which other terms occur, emerge when first-order radiation boundary condition or conductivity losses are considered. For these kind of problems, the system poles are the eigenvalues of a polynomial eigenproblem or, in the more general case, a rather nonlinear eigenproblem. While there are numerical techniques that can find these eigenpairs [38], the orthogonality of the eigenvectors is lost. This is a serious limitation as orthogonality is essential for splitting and separating the regular part of the impedance matrix transfer function from the singular one.

Alternatively, radiation or scattering problems can be analyzed using the proposed SSMM-MOR technique with spherical mode expansion [39]. This obviously imposes some limitations on the type of open structures that can be treated. Note that other techniques in which eigenfunction expansion is used—such as resonant mode expansion (RME), boundary integral resonant mode expansion (BI-RME) [40], [41], finite-integration technique (FIT) with two-step Lanczos reduction [42], and CRBM [22]—all possess similar limitations. Additional ports or approximate formulas can also be considered, as postulated in [43].

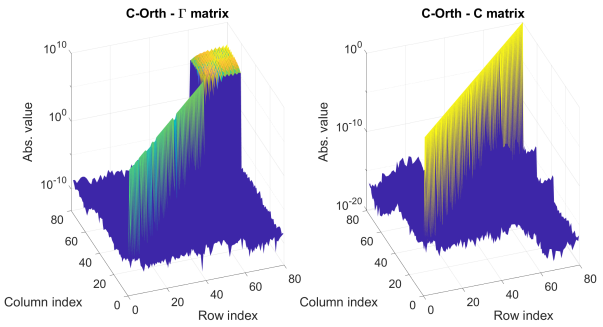

Fig. 5: Folded filter: ROM system matrices with C-orthonormalization.

VI. Numerical results

In this section, SSMM-MOR is used to perform a fast frequency sweep and compute the scattering parameters of four structures. All tests were implemented in a Matlab environment or C++ code using an Intel i5-7400 processor and 64GB RAM. Intel MKL PARDISO [27] was used to solve large systems of linear equations. The error tolerance was taken as 1e-4 in all cases. The reference scattering and impedance matrices were computed using full-order model (equations: (4) and (5), respectively).

A. Folded waveguide filter

In the first test, we used the method to analyze a folded filter, as considered in previous sections. It was first analyzed using the original FEM formulation [29] with 359,202 unknowns in the 12–24 GHz band, at 2001 points. In order to accurately model the structure, all the modes excited in the band of interest have been considered, giving $n_m = 10$ (five modes for each port). The results are presented in Fig. 1.

Next, the reduction scheme described in this paper was applied. In order to approximate the singular part of the impedance function, we generated a projection basis $\mathbf{Q}_E$ composed of the 51 eigenvectors associated with the resonant frequencies in the 12–24 GHz band. To approximate the

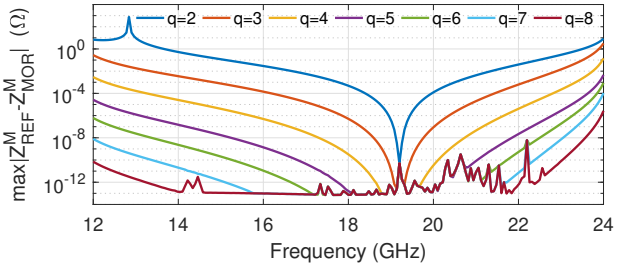

Fig. 6: The error between the original regular part of the impedance and the reduced part as a function of the number of block moments in the projection basis, where q indicates the number of block moments.

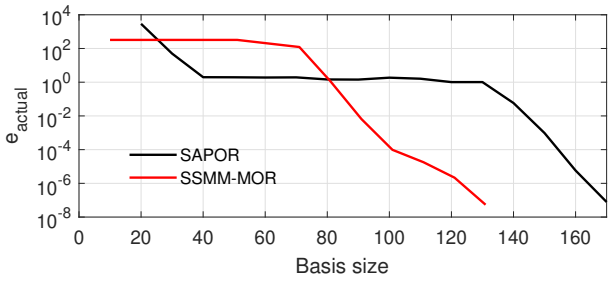

Fig. 7: Maximum value of the actual error as a function of the number of vectors in the projection basis for the folded waveguide filter.

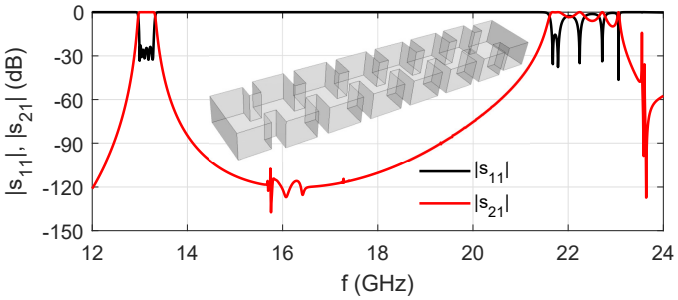

Fig. 8: Scattering parameters of H-plane filter.

regular space, the projection basis $\mathbf{Q}_M$, consisting of just eight block moments, has been computed using the procedures described in section V. The error estimator serves as stopping criterion. Since we have enforced C-orthogonalization of the regular and singular part of the projection basis $\mathbf{Q} = [\mathbf{Q}_E\ \mathbf{Q}_M]$, we obtain the decoupled reduced matrices $\mathbf{\Gamma}_R^d$ and $\mathbf{C}_R^d$, which is consistent with the theory provided in equations (19)–(30), and can be seen in Fig. 5. Fig. 4 shows the plots of the original, regular, and singular parts of the impedance. Fig. 6 shows the error between the original regular part of the impedance and the reduced part, as a function of the number of block moments in the projection basis. It can be seen that the error drops significantly with the reduction order. The final plot in Fig. 7 shows the maximum value of the actual error as a function of the size of the projection basis. In this case, 131 vectors sufficed to obtain the reduced-order model that accurately approximates the original model over the whole frequency band. Finally, we have performed the fast-frequency sweep using traditional SAPOR. It can be seen that, in this case, as many as 170 vectors are needed to generate the reduced model with an accuracy below $1e-4$, as shown in the results described in Section III. Table I summarizes these results of SAPOR and SSMM-MOR.

B. H-plane filter

The second test deals with a H-plane filter based on the WR-75 waveguide [44]. The goal of the simulation was to compute the scattering parameters of the structure in the 12–24 GHz band at 401 equidistantly located points, with eight modes excited at each of the ports. Firstly, the original FEM model with 162,200 unknowns was generated, and the reference scattering characteristics were computed. In order to accurately model the structure, all the modes excited in the band of interest have been considered, giving $n_m = 16$ (eight modes for each port). The results are presented in Fig. 8.

TABLE I: Analysis results for the folded waveguide filter, $n_m = 10$

Algorithm	SAPOR	SSMM-MOR
No. of eigenvectors	-	51
No. of moments	17	8
Total basis size	170	131

Next, SSMM-MOR was used to perform the fast frequency sweep. Solving for the eigenvectors, the 75 eigenresonances were found in the specified band. In order to uplift the projection basis, eight block moments were generated to approximate the regular subspace.

The plot of the singular impedance component associated with the fundamental port mode (wave mode with the lowest cutoff frequency) is shown in Fig. 9; it can be observed that it is highly nonlinear. On the other hand, the regular impedance component is smooth, as expected. We obtained ROM with a size if 203, where the traditional SAPOR approach needed as many as 288 vectors to achieve the same level of estimated error; this is shown in Fig. 9.

C. Eighth-order dual mode waveguide filter

In the third test, we analyzed an eighth-order dual mode waveguide filter [45], considering the 11–19 GHz frequency band with 201 equidistant points. In the first simulation, the scattering parameters of the filter were obtained using the original FEM model with 202,474 unknowns. All the modes excited in the band of interest have been considered, resulting in $n_m = 16$ (8 modes for each port). The results, as well as the geometry of the filter, are presented in Fig. 10.

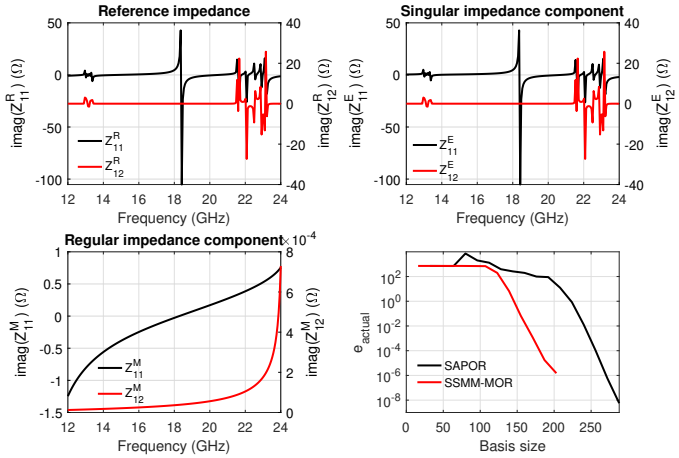

Fig. 9: H-plane filter: reference impedance plot, singular impedance component, regular impedance component, and maximum value of the actual error as a function of the number of vectors in the projection basis for SSMM-MOR and SAPOR.

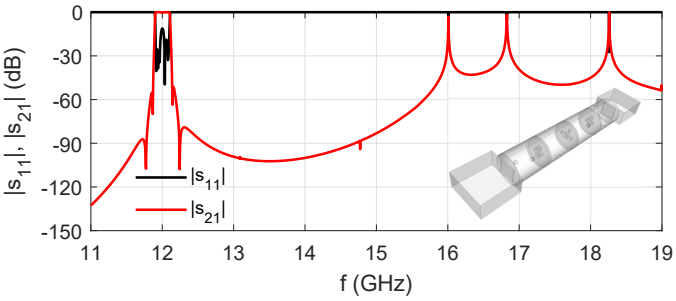

Fig. 10: Scattering parameters of a dual mode filter.

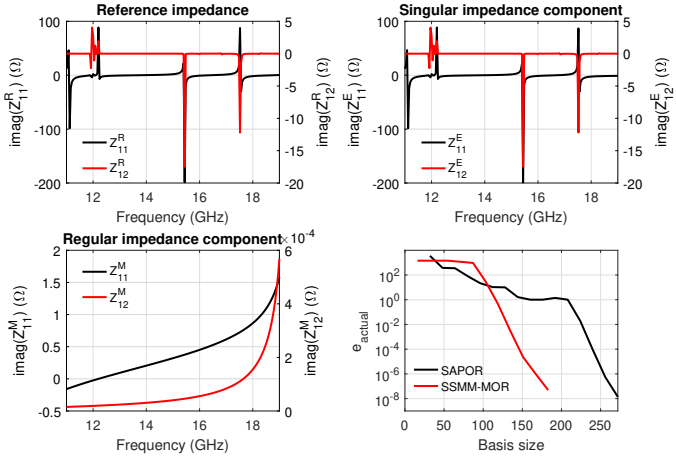

Fig. 11: Eighth-order dual mode filter: reference impedance plot, singular impedance component, regular impedance component, and maximum value of the actual error as a function of the number of vectors in the projection basis for SSMM-MOR and SAPOR.

In the next step, the proposed reduction scheme was applied. In order to approximate the singular subspace, 55 eigenvectors associated with poles in the specified frequency band were computed; the regular part of the projection basis consists of 8 block moments. Thus, the size of the entire basis is 183, while the traditional SAPOR approach needed 272 vectors to achieve the same level of error. A comparison of the two methods, along with the reference impedance plot, singular impedance component, and regular impedance component as a function of frequency, is shown in Fig. 11.

D. Dielectric resonator bandpass filter

The last test dealt with a lossy structure: a dielectric resonator filter [46] analyzed at 201 frequency points in the 4–12 GHz frequency band. The filter contains dielectric rings with $\epsilon_r = 38$ and a dielectric loss tangent of 1e-3. The reference characteristics were obtained using the model with 219,326 unknowns. The scattering parameters, as well as the geometry of the filter, are presented in Fig. 12.

Since the structure contains a lossy dielectric material, the formulas provided in Section V-B have to be utilized in order to construct the projection basis. The singular subspace consists of 101 eigenvectors, while the regular part is constructed with 14 block moments. Thus, the size of the

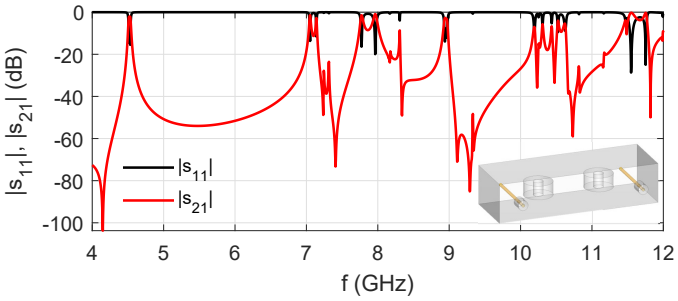

Fig. 12: Scattering parameters and geometry of dielectric resonator filter.

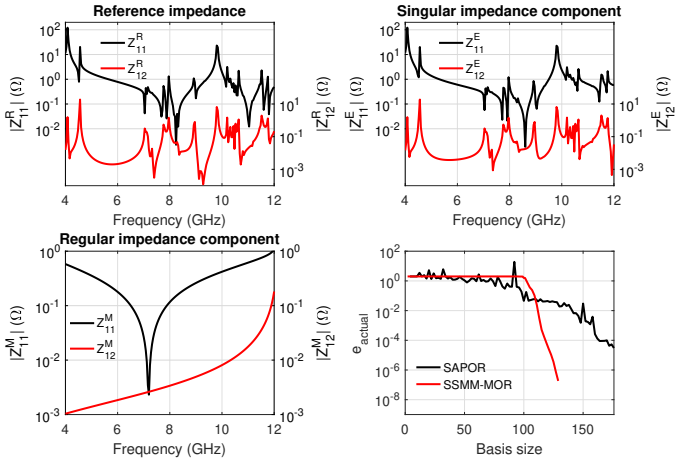

Fig. 13: Dielectric resonator filter: reference impedance plot, singular impedance component, regular impedance component, and the maximum value of the actual error as a function of the number of vectors in the projection basis for SSMM-MOR and SAPOR.

whole basis is 129, whereas the traditional SAPOR approach needed 176 vectors to achieve the same level of estimated error. A comparison of both SAPOR and SSMM-MOR methods, along with the reference impedance plot, singular impedance component, and regular impedance component as a function of frequency, is shown in Fig. 13.

E. The size of the reduced-order models

In the last test, we would like to compare the size of the reduced-order models obtained by means of the proposed SSMM-MOR method, with other MOR techniques, namely: RBM, SAPOR, CRBM and RGM-MOR [15]. It is assumed that the accuracy of all ROMs is the same – the maximum value of estimated error is below 1e-4. Table II summarizes the results. It can be seen that for all the cases considered, CRBM allows one to generate the most compact ROM. The size of ROMs obtained by means of SSMM-MOR is slightly larger (less than 20%).

F. Runtime comparison

In the last numerical test we would like to characterize the efficiency of the proposed approach, compared to other MOR

TABLE II: The size of reduced-order models generated using RBM, SAPOR, SSMM-MOR, CRBM, RGM-MOR

Algorithm	Case A	Case B	Case C	Case D
RBM	160	256	224	120
SAPOR	170	288	272	176
SSMM-MOR	131	203	183	129
CRBM	111	171	151	115
RGM-MOR	190	400	304	150

TABLE III: Runtimes of RBM, SAPOR, SSMM-MOR, CRBM, RGM-MOR

	A	B	C	A2	B2	C2
RBM	138.9s	107.6s	76.4s	14.7s	5.7s	10.5s
SAPOR	132.7s	179.8s	144.8s	**8.9**s	**3.6**s	5.5s
SSMM-MOR	121.1s	**76.1**s	**64.9**s	11.7s	4.9s	7.7s
CRBM	126.9s	84.5s	69.6s	13.9s	4.9s	10.8s
RGM-MOR	**91.5**s	189.7s	104.5s	**8.9**s	**3.6**s	**5.3**s

methods: CRBM, RBM, SAPOR and RGM-MOR. All these methods comprise algorithmic steps such as: factorization, solution of FEM system of equations, projection of the FEM matrices onto a subspace spanned by the projection basis, error estimation and orthogonalization of the projection basis. The computational complexity depends not only on FEM degrees of freedom n but also on the number of frequency points n_f, the number of vectors in projection basis v and the number of RHS (right-hand side) vectors n_m. Moreover, factorization, solution and projection involve operations performed on sparse matrices. Sparse matrix solution kernels are difficult to be characterized in terms of numerical complexity as this heavily depends on the number of nonzero elements and sparsity pattern, among others. Therefore, instead of comparing the computational complexity, we compare runtimes of five MOR techniques for selected simulation scenarios using C++ code. To this end, we consider six cases: A, B, C (which have been analyzed in previous numerical tests) and A2, B2, C2, which are the same as A, B, C, with the only difference being the frequency band of interest (14-15GHz, 12.5-13.5GHz, and 11-13GHz, respectively).

The results are shown in Table III, where the shortest and the longest runtimes are denoted using bold and underline, respectively. It can be seen that for narrow frequency-band simulations (A2, B2, C2), moment-matching techniques (SAPOR and RGM-MOR) are the fastest, whereas methods which require a few FEM system matrix factorizations (RBM and CRBM) are less efficient. However, for the wideband simulations, the answer to the question: *which MOR method is the most efficient?* is not straightforward. The computational time of MOR algorithms depends not only on factors highlighted above, but also on other parameters such as the width of the frequency band, the number of times and the number of frequency points at which the error estimate is evaluated, the computing platform (processor, the number of threads, memory bandwidth), MOR accuracy, geometry of the structures, etc. However, what is apparent is that for wideband analysis, despite requiring only one single factorization, SAPOR seems to perform poorly. RGM-MOR is the fastest for case A, however, for cases B and C it is much slower, comparing to SSMM, CRBM and RBM. SSMM-MOR wins in cases B and C, and comes out second in case A. It also performs reasonable well in the narrowband tests. In all six tests the runtimes for SSMM-MOR are better than for RBM and CRBM (with the exception of a draw between CRBM and SSMM-MOR for case B2). So, while it is not always an optimal choice, SSMM-MOR certainly offers a significant speedup over SAPOR for multiport wideband analysis and decent performance for narrowband problems.

G. Computing Eigenvectors

In our implementation of CRBM and SSMM-MOR we use Arnoldi/Lanczos method (ARPACK library) in the shift and invert mode. The eigenvectors are computed iteratively. Each iteration requires the solution of the system of FEM equations. This is done using the factors obtained in the numerical factorization. The number of iterations depends on the number of eigenvectors required, the frequency band considered in the simulation, the number of variables, the geometry of a structure, etc. It is not easy to provide a general formula for the number of floating point operations of the symbolic and numerical factorizations, as well as the solve stage. In the previous section we provided runtimes for the complete process. In Table IV we give the number of numerical factorizations and solve operations used to generate the projection basis for each of the MOR algorithms. We consider two cases: narrowband and wideband analysis (A2 and A). The numbers in round brackets denote the number of solve operations used to compute the eigenvectors.

TABLE IV: Number of factorizations and solutions in CRBM and SSMM.

	Fact.	Solve	Fact.	Solve
Algorithm	Case A (10 RHS)		Case A2 (10 RHS)	
RBM	16	160	6	12
SAPOR	1	170	1	16
SSMM-MOR	1	182 (102)	1	26 (16)
CRBM	6	162 (102)	3	22 (16)
RGM	3	190	1	16

VII. Conclusions

This paper has proposed a novel model-order reduction approach for efficient wide frequency band FEM simulation of microwave components. This approach generates a projection basis composed of the eigenmodes hit in the frequency band of analysis and the subsequent block moments of the original system. This allows the system transfer function to be split into a singular and regular part. The regular part is then approximated by a few block moments, while the singular part is found by projecting the system matrices onto a space spanned by the eigenvectors corresponding to the poles located within the frequency band of interest. The results show that this method is a cost-effective alternative to state-of-the-art MOR techniques, especially when the time needed to factorize the FEM system matrix becomes dominant.

One restriction of the method proposed in this paper is that the two subspaces need to be orthogonal in the energy sense

(or strictly speaking, the pseudoenergy sense). In practical terms this means that either the structure is lossless or the loss can be expressed in terms of a frequency-independent (but possibly complex) permittivity or permeability.

ACKNOWLEDGEMENT

The authors would like to thank Prof. A. Lamecki and EMinvent company for providing a finite element method code (InventSim) which was used in the research reported in this paper.

REFERENCES

[1] Y. Ding, K.-L. Wu, and D. G. Fang, "A broad-band adaptive-frequency-sampling approach for microwave-circuit EM simulation exploiting Stoer-Bulirsch algorithm," *IEEE Trans. Microw. Theory Techn.*, vol. 51, no. 3, pp. 928–934, Mar. 2003.

[2] R. S. Adve, T. K. Sarkar, S. M. Rao, E. K. Miller, and D. R. Pflug, "Application of the Cauchy method for extrapolating/interpolating narrowband system responses," *IEEE Trans. Microw. Theory Techn.*, vol. 45, no. 5, pp. 837–845, May 1997.

[3] D. Deschrijver, T. Dhaene, and D. De Zutter, "Robust parametric macromodeling using multivariate orthonormal vector fitting," *IEEE Trans. Microw. Theory Techn.*, vol. 56, no. 7, pp. 1661–1667, Jul. 2008.

[4] G. Antonini, D. Deschrijver, and T. Dhaene, "Broadband rational macromodeling based on the adaptive frequency sampling algorithm and the partial element equivalent circuit method," *IEEE Trans. Electromagn. Compat.*, vol. 50, no. 1, pp. 128–137, Feb. 2008.

[5] T. Dhaene, J. Ureel, N. Fache, and D. De Zutter, "Adaptive frequency sampling algorithm for fast and accurate S-parameter modeling of general planar structures," in *Proc. IEEE MTT-S Symp. Dig.* IEEE, 1995, pp. 1427–1430.

[6] S. Lefteriu and A. C. Antoulas, "A new approach to modeling multiport systems from frequency-domain data," *IEEE Trans. Comput.-Aided Design Integr. Circuits Syst.*, vol. 29, no. 1, pp. 14–27, Jan. 2010.

[7] V. de la Rubia, U. Razafison, and Y. Maday, "Reliable fast frequency sweep for microwave devices via the reduced-basis method," *IEEE Trans. Microw. Theory Techn.*, vol. 57, no. 12, pp. 2923–2937, Dec. 2009.

[8] M. Rewienski, A. Lamecki, and M. Mrozowski, "A goal-oriented error estimator for reduced basis method modeling of microwave devices," *IEEE Microw. Wireless Compon. Lett.*, vol. 25, no. 4, pp. 208–210, Apr. 2015.

[9] Y. Su, J. Wang, X. Zeng, Z. Bai, C. Chiang, and D. Zhou, "SAPOR: second-order Arnoldi method for passive order reduction of RCS circuits," in *Proc. Int. Conf. Comput.-Aided Design (ICCAD)*. IEEE Computer Society, Nov. 2004, pp. 74–79.

[10] B. N. Sheehan, "ENOR: Model order reduction of RLC circuits using nodal equations for efficient factorization," in *Proc. IEEE 36th Design Autom. Conf.* ACM, Jun. 1999, pp. 17–21.

[11] L. T. Pillage, R. Rohrer *et al.*, "Asymptotic waveform evaluation for timing analysis," *IEEE Trans. Comput.-Aided Design Integr. Circuits Syst.*, vol. 9, no. 4, pp. 352–366, Apr. 1990.

[12] L. Feng, J. G. Korvink, and P. Benner, "A fully adaptive scheme for model order reduction based on moment matching," *IEEE Trans. Compon. Packag. Manuf. Technol.*, vol. 5, no. 12, pp. 1872–1884, Dec. 2015.

[13] T.-S. Nguyen, T. Le Duc, T.-S. Tran, J.-M. Guichon, O. Chadebec, and G. Meunier, "Adaptive multipoint model order reduction scheme for large-scale inductive PEEC circuits," *IEEE Trans. Electromagn. Compat.*, vol. 59, no. 4, pp. 1143–1151, Aug. 2017.

[14] M. Rewienski, A. Lamecki, and M. Mrozowski, "Greedy multipoint model-order reduction technique for fast computation of scattering parameters of electromagnetic systems," *IEEE Trans. Microw. Theory Techn.*, vol. 64, no. 6, pp. 1681–1693, Jun. 2016.

[15] G. Fotyga, M. Czarniewska, A. Lamecki, and M. Mrozowski, "Reliable greedy multipoint model-order reduction techniques for finite-element analysis," *IEEE Antennas Wireless Propag. Lett.*, vol. 17, no. 5, pp. 821–824, May 2018.

[16] R. D. Slone and R. Lee, "Applying Padé via Lanczos to the finite element method for electromagnetic radiation problems," *Radio Sci.*, vol. 35, no. 2, pp. 331–340, Mar. 2000.

[17] R. D. Slone, R. Lee, and J.-F. Lee, "Multipoint Galerkin asymptotic waveform evaluation for model order reduction of frequency domain FEM electromagnetic radiation problems," *IEEE Trans. Antennas Propag.*, vol. 49, no. 10, pp. 1504–1513, Oct. 2001.

[18] M. Jemai and A. B. Kouki, "New adaptive multi-expansion frequencies approach for SP-MORe techniques with application to the well-conditioned asymptotic waveform evaluation," *IEEE Trans. Microw. Theory Techn.*, vol. 65, no. 10, pp. 3709–3719, Oct. 2017.

[19] R. D. Slone, R. Lee, and J.-F. Lee, "Well-conditioned asymptotic waveform evaluation for finite elements," *IEEE Trans. Antennas Propag.*, vol. 51, no. 9, pp. 2442–2447, Sep. 2003.

[20] A. Odabasioglu, M. Celik, and L. T. Pileggi, "PRIMA: passive reduced-order interconnect macromodeling algorithm," in *Proc. IEEE/ACM Int. Conf. Computer-Aided Design*. IEEE Computer Society, Aug. 1997, pp. 58–65.

[21] B. Liu *et al.*, "Block SAPOR: Block second-order Arnoldi method for passive order reduction of multi-input multi-output RCS interconnect circuits," in *Proc. IEEE Asia South Pacific Design Autom. Conf.*, vol. 1, Jan. 2005, pp. 244–249.

[22] V. de la Rubia and M. Mrozowski, "A compact basis for reliable fast frequency sweep via the reduced-basis method," *IEEE Trans. Microw. Theory Techn.*, vol. 66, no. 10, pp. 4367–4382, Oct. 2018.

[23] D. Szypulski and G. Fotyga, "Second-order Arnoldi method for wideband fast frequency sweeps," *presented at IEEE Int. Numer. Electromagne. Modeling Optim. Conf., Boston, USA*, May 29-31, 2019.

[24] J.-M. Jin, *The Finite Element Method in Electromagnetics*, 3rd ed. New Jersey: John Wiley & Sons, 2014.

[25] J. Schöberl, "NETGEN An advancing front 2D, 3D-mesh generator based on abstract rules," *Computing and visualization in science*, vol. 1, no. 1, pp. 41–52, 1997.

[26] P. Ingelstrom, "A new set of H (curl)-conforming hierarchical basis functions for tetrahedral meshes," *IEEE Trans. Microw. Theory Techn.*, vol. 54, no. 1, pp. 106–114, Jan. 2006.

[27] O. Schenk and K. Gärtner, "Solving unsymmetric sparse systems of linear equations with PARDISO," *Future Gener. Comput. Syst.*, vol. 20, no. 3, pp. 475–487, Apr. 2004.

[28] A. Lamecki, "A mesh deformation technique based on solid mechanics for parametric analysis of high-frequency devices with 3-D FEM," *IEEE Trans. Microw. Theory Techn.*, vol. 64, no. 11, pp. 3400–3408, Nov. 2016.

[29] A. Lamecki, L. Balewski, and M. Mrozowski, "An efficient framework for fast computer aided design of microwave circuits based on the higher-order 3D finite-element method," *Radioengineering*, vol. 23, no. 4, pp. 970–978, Dec. 2014.

[30] M. Hess and P. Benner, "Fast evaluation of time harmonic Maxwell's equations using the reduced basis method," *IEEE Trans. Microw. Theory Techn.*, vol. 61, no. 6, pp. 2265–2274, Jun. 2013.

[31] W. Wang, G. N. Paraschos, and M. N. Vouvakis, "Fast frequency sweep of FEM models via the balanced truncation proper orthogonal decomposition," *IEEE Trans. Antennas Propag.*, vol. 59, no. 11, pp. 4142–4154, Nov. 2011.

[32] A. Sommer, O. Farle, and R. Dyczij-Edlinger, "A new method for accurate and efficient residual computation in adaptive model-order reduction," *IEEE Trans. Magn.*, vol. 51, no. 3, pp. 1–4, Mar. 2015.

[33] M. W. Hess, S. Grundel, and P. Benner, "Estimating the inf-sup constant in reduced basis methods for time-harmonic Maxwell's equations," *IEEE Trans. Microw. Theory Techn.*, vol. 63, no. 11, pp. 3549–3557, Nov. 2015.

[34] Y. Saad, *Numerical methods for large eigenvalue problems: revised edition*. Siam, 2011, vol. 66.

[35] Z. Bai and Y. Su, "SOAR: A second-order Arnoldi method for the solution of the quadratic eigenvalue problem," *SIAM J. Matrix Anal. Appl.*, vol. 26, no. 3, pp. 640–659, 2005.

[36] R. B. Lehoucq, D. C. Sorensen, and C. Yang, *ARPACK users' guide: solution of large-scale eigenvalue problems with implicitly restarted Arnoldi methods*. Siam, 1998, vol. 6.

[37] L. Feng, A. C. Antoulas, and P. Benner, "Some a posteriori error bounds for reduced-order modelling of (non-) parametrized linear systems," *ESAIM: Mathematical Modelling and Numerical Analysis*, vol. 51, no. 6, pp. 2127–2158, 2017.

[38] J. E. Roman, C. Campos, E. Romero, and A. Tomás, "SLEPc users manual," *D. Sistemes Informàtics i Computació Universitat Politècnica de València, Valencia, Spain, Report No. DSIC-II/24/02*, 2015.

[39] V. de la Rubia and J. Zapata, "MAM–A multipurpose admittance matrix for antenna design via the finite element method," *IEEE Trans. Antennas Propag.*, vol. 55, no. 8, pp. 2276–2286, Aug. 2007.

[40] P. Arcioni, M. Bozzi, M. Bressan, G. Conciauro, and L. Perregrini, "The BI-RME method: An historical overview," in *Proc. 2014 Int. Conf. Numer. Electromagn. Model. Optim. RF, Microw., Terahertz Appl.* IEEE, May 2014, pp. 1–4.
[41] G. Conciauro, P. Arcioni, M. Bressan, and L. Perregrini, "Wideband modeling of arbitrarily shaped H-plane waveguide components by the "boundary integral-resonant mode expansion method"," *IEEE Trans. Microw. Theory Techn.*, vol. 44, no. 7, pp. 1057–1066, Jul. 1996.
[42] T. Wittig, R. Schuhmann, and T. Weiland, "Model order reduction for large systems in computational electromagnetics," *Linear Algebra and Its Appl.*, vol. 415, no. 2-3, pp. 499–530, 2006.
[43] M. Bozzi, L. Perregrini, and K. Wu, "Modeling of conductor, dielectric, and radiation losses in substrate integrated waveguide by the boundary integral-resonant mode expansion method," *IEEE Trans. Microw. Theory Techn.*, vol. 56, no. 12, pp. 3153–3161, Dec. 2008.
[44] J. A. Ruiz-Cruz, J. R. Montejo-Garai, and J. M. Rebollar, "Computer aided design of waveguide devices by mode-matching methods," in *Passive Microwave Components and Antennas*. InTech, Apr. 2010, pp. 117–140.
[45] V. de la Rubia, "Reliable reduced-order model for fast frequency sweep in microwave circuits," *Electromagnetics*, vol. 34, no. 3-4, pp. 161–170, 2014.
[46] J. R. Brauer and G. C. Lizalek, "Microwave filter analysis using a new 3-D finite-element modal frequency method," *IEEE Trans. Microw. Theory Tech.*, vol. 45, no. 5, pp. 810–818, May 1997.

Damian Szypulski (S'19) received the M.S.E.E. degree in microwave engineering from the Gdańsk University of Technology, Gdańsk, Poland, in 2018, where he is currently pursuing the Ph.D. degree at the Department of Microwave and Antenna Engineering.

His current research interests include computational electromagnetics, mainly focused on the finite-element method and model-order reduction techniques for the analysis of microwave devices.

PLACE PHOTO HERE

Grzegorz Fotyga (M'19) received M.S.E.E. and Ph.D. degrees in electronic engineering from Gdańsk University of Technology in 2009 and 2016. He is currently Assistant Professor with the Department of Microwave and Antenna Engineering, Gdańsk University of Technology. His current research interests include computational electromagnetics, numerical methods, the finite element method, and model order reduction.

Valentín de la Rubia received the Ingeniero de Telecomunicación and Ph.D. degrees from the Universidad Politécnica de Madrid, Madrid, Spain, in 2003 and 2008, respectively.

He was an Assistant Professor with the Universidad de Oviedo, Asturias, Spain, from 2007 to 2008, and with the Universidad de Extremadura, Extremadura, Spain, from 2008 to 2011. Since 2011, he has been an Assistant Professor with the Universidad Politécnica de Madrid.

His current research interests include computational electromagnetics and model-order reduction techniques for microwave circuit and antenna design.

PLACE PHOTO HERE

Michal Mrozowski (S'88–M'90–SM'02–F'08) received the M.Sc. and Ph.D. degrees from the Gdańsk University of Technology, Gdańsk, Poland, in 1983 and 1990, respectively. In 1986, he joined the Faculty of Electronics, Gdańsk University of Technology, where he is currently a Full Professor and the Head of the Department of Microwave and Antenna Engineering. His current research interests include computational electromagnetics, GPU computing, CAD of microwave devices, filter design, and optimization techniques.